A Portable Chemical Detection System with Anti-body Biosensor for Impedance Based Monitoring of T2-mycotoxin Bioterrorism Agents

V. I. Ogurtsov(✉) and K. Twomey

Tyndall National Institute, Lee Maltings, University College Cork, Cork, Ireland
vladimir.ogurtsov@tyndall.ie

Abstract. The work describes the development of a portable and autonomous biosensing label free platform for detection of biotoxin substances. The biosensor is realized as an on-chip package-free micro electrochemical cell consisting of a counter electrode (CE), a reference electrode (RE) and a working electrode (WE) patterned on a single silicon chip. To improve sensor sensitivity, the WE was implemented as a microelectrode array of 40 micron diameter gold disks with 400 micron centre-to-centre distance, which underwent corresponding surface modification for antibody immobilisation. The interfacial biosensor changes produced by T2-mycotoxin antigen-antibody reaction were sensed by means of Electrochemical Impedance Spectroscopy in a frequency range from 10 Hz to 100 kHz. The signal processing algorithm for mycotoxin quantification was based on analysis of biosensor impedance spectra and its equivalent electrical circuit. It is implemented in corresponding software at microcontroller and single-board computer level in such a manner that the results can be produced at point-of-need or in the decision center without user intervention. The instrumentation represented a mix signal measurement system which consisted of analog and digital parts. The analog part constituted a low noise, highly-sensitive hardware which implemented impedance measurements on the basis of a quadrature signal processing of the biosensor in response to a harmonic stimulation signal. The key unit of the digital part of the device was an Atmel microcontroller with inbuilt 12-bit ADC and external 16-bit DAC, which are responsible for device configuration, stimulation signal generation, biosensor signal digitalization, its initial signal processing and communication with the single-board computer. A calibration of the platform in the range of 0–250 ppm of T2 toxin concentrations confirmed that the system can provide successful detection of the toxin at the levels above 25 ppm.

Keywords: Label-free biosensor · T2-mycotoxin · Immunosensor
Surface modification · Electrochemical Impedance Spectroscopy
Portable instrumentation · Equivalent circuit · Signal processing

N. Peixoto et al. (Eds.): BIOSTEC 2017, CCIS 881, pp. 45–73, 2018.
https://doi.org/10.1007/978-3-319-94806-5_3

1 Introduction

The development of miniaturized, portable biosensing systems for the rapid, reliable and low cost determination of contaminating bio agents in the environment (atmosphere, water, food etc.) has received considerable attention in recent years particularly with the advancements in biotechnology. In the last decade with the growing threat of bioterrorism, the demand on development of systems that can rapidly and accurately detect bio agents, that can threaten human life or health, is significantly increased. There exist a few options for the detection of bioterrorism agents [1]:

1. Generic detectors that provide an on/off alert
2. Biosensors for rapid screening and presumptive identification [2, 3] and
3. Identification systems for definitive confirmation.

Of the three technologies, biosensors can play an important role in detection of Chemical, Biological, Radiological, Nuclear, and Explosive (CBRNE) materials because they can provide a sensitive monitoring tool whilst also being amenable to miniaturization and forming part of a portable system. Beside security, biosensing systems are increasingly used in a range of other different applications including environmental, clinical, food and agriculture [4–15]. The conventional approaches are mainly lab-based and cannot be easily deployed at point-of-need. Modern microfabricated biosensors, on the other hand, offer the advantages of a cost-effective and rapid sample analysis, and specific and sensitive measurements over the traditional methods, which tend to be a multi-step (e.g. ELISA), or to involve sophisticated and expensive equipment (e.g. HPLC). The ability to apply semiconductor processing technologies, more commonly used in the IC industry, in the sensor chip fabrication [8, 10] enables large batch production and subsequent availability of cheap and disposable devices.

The International Union of Pure and Applied Chemistry (IUPAC) defines a biosensor as follows "A biosensor is a self-contained integrated device which is capable of providing specific quantitative or semi-quantitative analytical information using a biological recognition element (biochemical receptor) that is in direct spatial contact with a transducer element" [11, 12]. Thus, according to this classification a biosensor is essentially composed of two elements:

1. A bioreceptor that is an immobilized sensitive biological element (e.g. enzyme, DNA, antibody) recognizing the analyte (e.g. enzyme substrate, complimentary DNA, antigen).
2. A transducer that converts (bio) chemical signal resulting from the interaction of the analyte with the bioreceptor into its electrical equivalent. The intensity of the signal generated is either directly or indirectly proportional to the analyte concentration.

Essentially, the selectivity or specificity of the biosensor depends on the biorecognition element, which is capable of "sensing" the presence of an analyte [13, 14]. There are currently three generations of biosensors in existence. The term generation was originally created to describe the stages of integration in biosensors. Biosensors with mediated response mainly generated by membrane-bound or membrane entrapped biocomponents (first generation), were followed by virtually

reagentless biosensors where biocomponents are fixed directly to the sensor surface and either the reaction of coimmobolised cosubstrates (bound to the electrode, polymer or enzyme itself) or the direct heterogeneous electron transfer between the prosthetic group and the electrode is exploited (second generation). While the immobilisation of the receptors directly on an electronic circuit leads to systems with integrated signal generation, transduction and processing (third generation) having the potential of considerable miniaturisation [15]. The devices investigated in this study should be considered as the third generation under this classification and this highlights the progress sensing systems since their relatively recent development.

Antibody-based biosensors or immunosensor are found on an antigen-antibody interaction where antibody (Ab), Y-shaped proteins, bind with a target, an invading antigen (Ag), through a high affinity binding reaction. The specificity of the reaction is due to a chemical constitution of antibody which is specific to the target antigen that defines similarity of the antigen-antibody reaction to a lock (antibody) and key (antigen) operation. This conditions such advantages of immunosensors as high versatility, selectivity, stability and sensitivity. At the same time, the strong antigen-antibody binding makes it very difficult to break these bonds, thus, a typical immunosensor is a disposable one-shot sensor that cannot be used after the target detection [16–20].

Immunosensors utilizing antibody-based recognition elements, have been developed on a wide range of transduction platforms. The transducer element translates the selective recognition of the analyte into a quantifiable signal and thus, has major influence on sensitivity [21]. Since 1959 when an antibodies based biosensor for the first time was used with radiolabeled assay for detection of insulin in the body fluids [22] immunosensors have revolutionized impact on detection of a whole lot of different target analytes such as disease markers, food and environmental contaminants, biological warfare agents and illicit drugs. Nowadays, transduction approaches used with immunosensors include electrochemical, piezoelectric and optical systems [15, 23] where the mostly used methods are based on optical and electrochemical methodology. However, the classical optical transduction mechanism has suffered from poor sensitivity when coupled with radioimmunoassay, the short half-life of radioactive agents, concerns of health hazards, and disposal problems. As well the optical methods usually require a complicated sample preparation that increases risk of sample contamination, rises cost and time of analysis and makes them difficult for implementation in a portable device capable of working in field conditions outside of specialized labs. Electrochemical detection overcomes the most of these problems and provides means for fast, simple, reliable and economical realization of portable autonomous immunosensing systems capable of working at point-of-need without end-user intervention [19, 24]. The advantage of electrochemical biosensors is also that they can monitor bimolecular interactions in real time. In this process the biorecognition components are immobolised on a solid surface (usually the sensor chip), and the component to be detected is present in the solution phase [25].

A typical electrochemical biosensor usually represents an electrode or an array of microdiscs/bands with corresponding bio functionalization acting as the working electrode within a three-electrode electrochemical cell containing also a reference electrode (i.e. Ag/AgCl) and an auxiliary/counter electrode (which varies) [26]. The working electrode provides the sensing capability, the reference and the counter electrodes

facilitate the measurements. A design option for the electrochemical biosensor is a bio specific membrane that selectively interacts with the analyte. A physical transducer coupled to the membrane detects this biointeraction and generates the resulting electrical signal. The bio specific membrane can be made up of a material that undergoes electron exchange reactions with the analyte so a direct electrical output signal consisting of a potential or a current can be detected and interpreted [27].

Typical microfabricated biosensors incorporate a gold electrode, or other materials e.g. platinum, Si_3N_4, active layer upon which different surface chemistries are applied to form a complete device that is specific and sensitive to a target of interest [28, 29]. Within the branch of electrochemical sensors, there are amperometeric, potentiometric, impedimetric and field-effect transistor (FET) biosensors [19, 23, 30, 31]. With the amperometric type biosensors, the sensor current is monitored with time; for the potentiometric – the voltage is monitored. Both of these types offer relatively straight forward measurements and a rapid analysis. The impedimetric is more complex and more sensitive technique. Its classical implementation is based on the measurement of an AC current that forms in the response on the application to the sensor a sinusoidal voltage over a set of frequencies. The advantage of impedemetric biosensor is that they can directly sense the changes in interface between the bio functionalized electrode and the sample solution due to the biorecognition reaction through monitoring of the sensor impedance variations. For that they do not need any additional labelling that is very often required in case of optical biosensor [22]. This circumstance along with relative simplicity of electrochemical instrumentation defines the ease and cheapness of impedemetric biosensors operation (no additional expensing labelling or sample preparation) that with such their advantages as high sensitivity and the ability to miniaturise the associated measurement instrumentation explains a growing interest in label-free impedimetric biosensors for different application [4, 32]. A further advance in electrochemical biosensors can be obtained by using of micro-sized electrodes, which improve the mass transport (and hence the sensor sensitivity) owing to the occurrence of radial diffusion over planar diffusion from macro-size electrodes resulting in an increase in the signal-to-noise ratio and reduction in the iR drop [33].

The presented study describes the development of such portable biosensing platform with immunosensor on the base of microfabricated microelectrode array capable of biotoxin detection. The performance of the platform was validated by detection of T2-toxin. It is a trichothecene mycotoxin, which is toxic to humans and animals. It is naturally occurring mould byproduct of Fusarium spp. fungus that can be found in grains such as barley, wheat and oats. It is well-known that some mycotoxins can be used as chemical warfare agents [34, 35]. Inside of this group, trichothecenes can act immediately upon contact, and exposure to a few milligrams of T-2 is potentially lethal. The symptoms exhibited by purported victims included internal hemorrhaging, blistering of the skin, and other clinical responses that are caused by exposure to trichothecenes.

Detection methods for T-2 toxin can be classified into two types: screening methods like ELISA and analytical methods like GC and HPLC [36, 37]. Since low ppb concentrations are usually required to be detected, very sensitive analytical methods are hence needed. Advantages of screening methods like ELISA are that these methods generally do not require a clean-up other than dilution of the extract and/or

filtration before analysis. ELISA type screening methods rely on antibodies to detect the T-2 toxin. The specific antibodies (monoclonal or polyclonal) distinguishes the 3D structure of T-2 toxin. Usually an incubation period of about 1-2 h is required to complete this bio recognition procedure. The T-2 toxin present in the sample being tested competes with a labelled toxin for a limited number of antibody binding sites. The more toxin in the sample solution, the lower the binding of the labelled toxin and the lower the signal generated by the assay. The presence of the T-2 toxin is indicated by a specific color change. However, there are disadvantages to this particular mechanism of detection. These two main disadvantages are high matrix dependence and overestimation of the T-2 toxin concentration, which can occur if structurally related mycotoxins or constituents present in the matrix interfere with the competitive antibody-binding site mechanism required for the detection of T-2 toxin by ELISA [38]. Hence, this could lead to false results. However, there are advantages of screening methods like ELISA. They are high sample throughput and ease of operation. Thus, detection limits of 0.1 ng/g obtained with this methodology have been reported [37]. Other recent screening methods include Molecularly Imprinted Polymers (MIPs) [38] and Dipstick and Lateral Flow tests, where detection limits of 4 and 50 ng/kg were stated [39].

The presented study describes the development of a portable autonomous impedimetric biosensing system with a label-free electrochemical immunosensor for T2-toxin detection for using at point of need. The immunosensor is based on a bio functionalized microelectrode array [24, 40] which works as a part of a microfabricated electrochemical cell realized as a single silicon packageless chip. The developed biosensing system played role of a biohazard detection unit in a portable HANHOLD platform developed for detection of CBRN threads for operating at point of need. The platform was created during fulfilment an FP7 collaborative project called Handhold (Handheld Olfactory Detector) [41] and included also an optical sensing module for detection of chemical thread (explosive) and a radioactivity detector. All modules were operating under integrated control from a single board PC that has possibility of wirelessly transmitting the platform data to an outside decision center. The platform was creating by the analogy of a sniffer dog that is used at airport custom control. While the dog will remain a central part of the detection process at border crossing and airports, sensor technology and low power computer based embedded system are improving to the extent that the time is now right to develop substantially improved mobile detection devices that can successfully complement the role played now mostly by dogs. Moreover, these detection devices can be networked together to provide enhanced alert facilities and also to enable easier management and field deployment of the platforms themselves.

2 Experimental

2.1 Description of the Bio Sensing System

The aim of the presented work was to develop a modular sensor platform which is reconfigurable and which can be deployed for a stand-off detection mimicking the

operational characteristics of a sniffer dog. Unlike the situation with dog retraining, this platform can be retargeted simply by removing one set of sensors and adding others, the software load reacting dynamically to the reconfiguration. Figure 1 illustrates the different technologies that play a role in the development of the Handhold biosensing system.

These technologies include microfabrication and surface chemistry that will be used for biosensor preparation, mix signal electronic design – for instrumentation hardware development, signal processing algorithm and corresponding software – for implementation of the autonomous system operation without end-user interference and integration – for completion of the system and providing its operability in the Handhold CBRN threads detection platform.

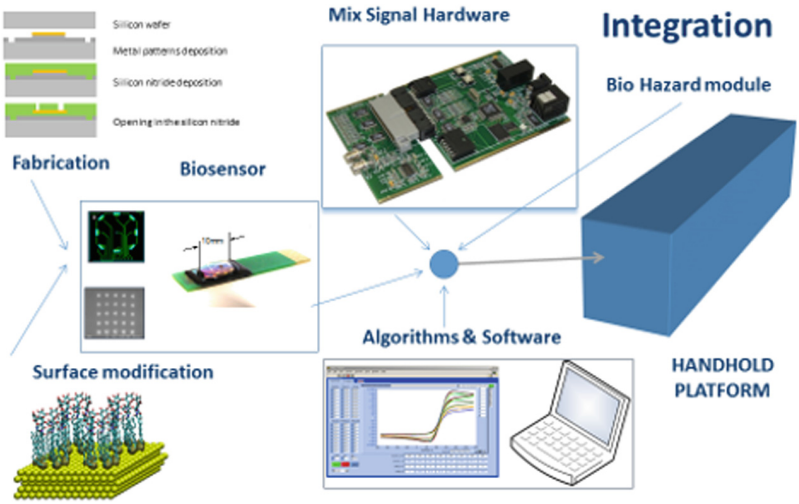

Fig. 1. The Handhold biosensing system.

2.2 Biosensor

As shown in Fig. 1 the biosensor consists of two main parts. They are a transducer (working electrode in the three-electrode micro electrochemical system) and a bio recognition layer that adds the bio specificity to the electrochemical sensor. For improving biosensor sensitivity a microelectrode array structure was selected for working electrode implementation. The development of the sensor transducer was started from simulation of different electrode designs including single disc, disc array, single band and band array. The simulation was performed in Multiphysics Engineering Simulation Software Comsol. The aim of this part of the work was to analyse the diffusion transport mechanism that occurs between the interface of the electrode and the sample solution and to determine the optimum transducer layouts according to its electrochemical performance. In this simulation, the model was created where each microelectrode was positioned at a set distance below the sensor surface. This was to

represent the physical fabrication process where an etch layer opens up areas of exposure in the top passivation layer to allow electrode contact with the environment. This technological process allows very fine electrode patterning but supposes that each electrode is located below the chip surface at the depth of few hundred of nm which is the range of possible thicknesses of the silicon nitride layer deposited on the metal. The hexagonal array configuration providing the most compact electrode placement [33] was considered with this simulation. For the disc array model, the diffusion zone approach was applied [42, 43], as schematically shown in Fig. 2.

The species concentration on the electrode surface was defined from the Nernst equation Eq. (1)

$$\frac{C_A}{C_B} = \exp\left(\frac{nF}{RT}\left(E - E^{/}\right)\right) \tag{1}$$

where C_A and C_B are concentrations of the electro active species involved into the electrochemical reaction, n is a number of electrons participated in electron exchange, R is the universal gas constant, F is the Faraday constant, $E^{/}$ is the formal potential. The electrode current was determined from integration of the diffusion flux over the electrode area, Eq. (2):

$$i = 2\pi nFD \int_0^{r_a} \left.\frac{\partial C(r,x,t)}{\partial x}\right|_{x=x_s} rdr \tag{2}$$

where D is diffusion coefficient of electro active species. Some results attained for the different electrode designs from this simulation are discussed below.

Examples of the calculated concentration profiles (occurring due to the diffusion mechanism taking place) at the different disc electrode structures and dimensions are shown in the diagrams presented in Fig. 3 in 10 s span after applying to the electrode a voltage that changes, according to Nernst equation Eq. (1), the concentration of the electro active species on the electrode surface to zero level.

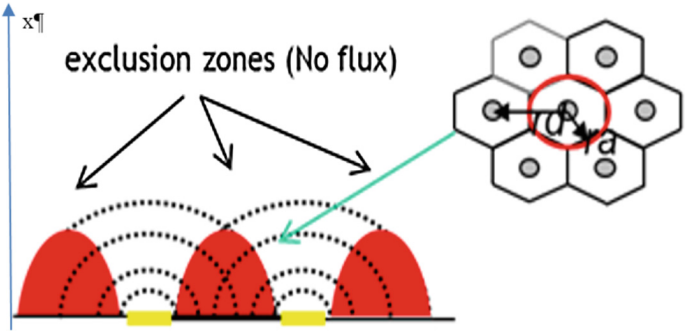

Fig. 2. Array model with the diffusion zone approach implemented.

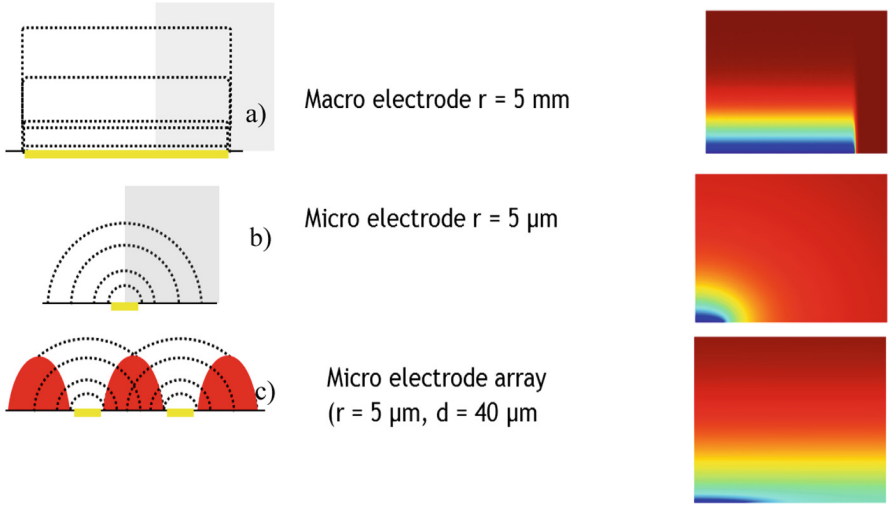

Fig. 3. Concentration profiles for macro, micro and micro electrode array after 10 s. (Color figure online)

As one can note, for a macro electrode, a planar type of diffusion occurs near the electrode (Fig. 3a). Diffusion zones can be seen in the changing color from blue to bright red. The dark red color situated at a distance from the electrode relates to the bulk concentration, where no or minimal diffusion is occurring. A reduction in electrode size from macro to micro changes the diffusion type from planar to radial. It can be seen by an example of a microelectrode of radius 5 µm that spans out a semicircular concentration wave from the electrode (Fig. 3b). This type of diffusion results in a high current density that leads to increase of signal to noise ratio, hence it is desirable to have. However, because of a small area of the microelectrode its total current is reduced in absolute value that can be difficult to measure in practice due to existence of electrochemical and electronic noises. To overcome this problem an array of microelectrodes can be used to increase the total signal. Care needs to be taken to ensure that there is no diffusion zones overlap between the neighboring electrodes. A general rule-of-thumb is to separate the electrodes in array by the length of more or equal to a specific center-to-center distance $d_c = 20r$ [44]. An example of overlapping diffusion zones is shown in Fig. 3c for a microdisc array of radius 5 µm and center-to-center distance of 40 µm (8 disc radii). As can be seen here, at a short distance from the array the concentration profiles transfer to the plain profile as in case of a macro electrode (Fig. 3a). This circumstance reduces the transducer signal. In order to avoid this situation, the center-to-center spacing in the transducer in the biosensor chip prototype for this disk radius was increased to 100 µm.

Dependence of the transducer current and current density from the time for the micro electrode array of different designs can be seen in Figs. 4 and 5. The current density of the whole electrode array is shown in the left plots and current of the whole electrode array is presented in the right plots of these figures. The transient process for a

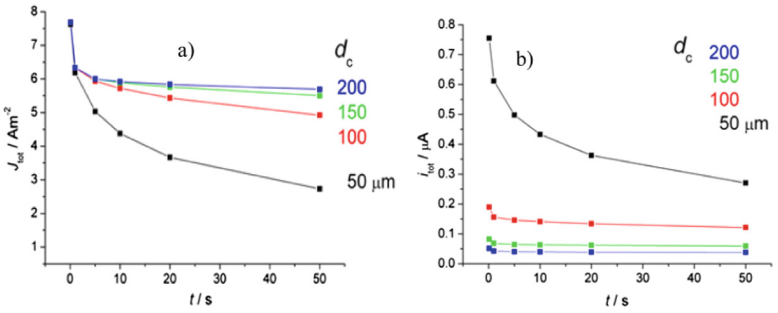

Fig. 4. Transient current density (a) and total current (b) for a microdisk electrodes array with r_a= 5 µm and different values of d_c and N_{el} as indicated in Table 1. (Color figure online)

time period of 50 s calculated for an array of microdisc electrodes of radius (r_e) of 5 µm and 1 µm with varying number of electrodes per array (N_{el}), center-to-center spacing (d_c), distance between electrode row (d_r) and the total electrode array area (S_A) as given in Table 1.

The results of the simulations show that for the largest center-to-center separation (blue curve) there is no or only slight interaction of the diffusion zones over the time span of 50 s and the current reaches a steady-state. The effect of diffusion zones overlap is two-fold. First, the current density is becoming smaller with decreasing center-to-center spacing values. Second, with decreasing d_c, the transients deviate from the steady state behavior. A complete overlap of the diffusion zones results in purely planar diffusion and the current starts to decrease at $t^{-1/2}$, as observed for macro electrodes and can be seen for the microdisc array of 5 µm radius and 50 µm center-to-center spacing in Fig. 4 and for the microdisc array of 1 µm radius and 10 µm center-to-center spacing Fig. 5.

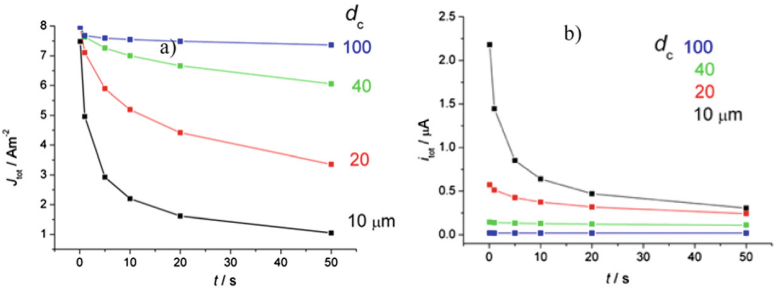

Fig. 5. Transient current density (a) and total current (b) for a microdisk electrodes array with r_a = 1 µm and different values of d_c and N_{el} as indicated in in Table 1.

As was mentioned above, due to the technological peculiarities after fabrication the microelectrode of radius r_e is located at the bottom of the pore in the isolation layer of thickness d_p deposited on the top of the metal. Thus, in the reality the microelectrode

Table 1. The electrode arrays geometrical parameters.

r_a, μm	d_c, μm	d_r, μm	N_{el}	S_A, m^2
5	200	170	85	6.676E−9
5	150	130	137	1.076E−8
5	100	86	314	2.466E−8
5	50	43	1260	9.896E−8
1	100	86.6	264	2.606E−9
1	40	34.6	1863	1.838E−8
1	20	17.3	7314	7.218E−8
1	10	8.7	29508	2.912E−7

represents a recessed electrode with aspect ratio $\gamma = d_p/r_e$ and performance of the microelectrode depends on this ratio. The simulation results for a single inlaid electrode and a recessed electrode with pore walls perpendicular to the electrode surface are shown in Figs. 6 and 7. Figure 6a demonstrates transient currents for an inlaid disk electrode (black curve) and for a recessed electrode with $\gamma = 0.2$ ($r_a = 5$ μm, $d_p = 1$ μm) (red curve) normalized to steady-state current of the inlaid electrode. Figure 6b shows dependence of the normalized steady-state current of the recess electrode as a function of the pore aspect ratio. Figure 7 presents the concentration profiles for the recess electrode at different times after application of the stimulation voltage: at 0.01 s - Fig. 7a, at 0.1 s - Fig. 7b, at 1 s - Fig. 7c and at 10 s - Fig. 7d. As can be seen from comparison of the inlaid and recess electrodes behavior the existence of the electrode recess leads to decrease of the steady-state current that can be quite significant for the large aspect ratio. From the concentration profiles follows that at start time (high frequencies) until concentration wave is inside of the pore the diffusion processes in a recess electrode are similar to macroelectrode behavior with a planar type of diffusion (Fig. 3a).

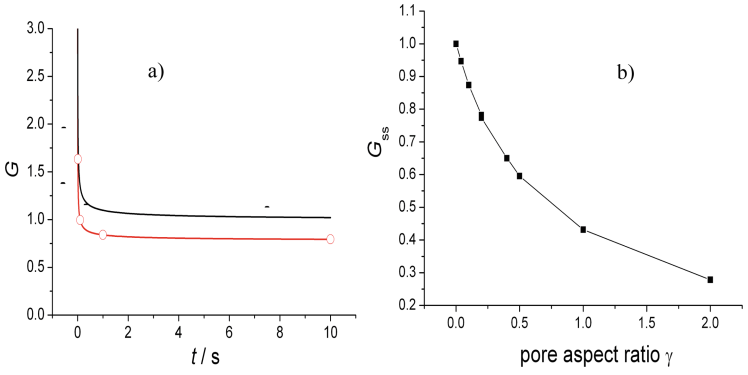

Fig. 6. Normalised transient current for an inlaid disk electrode (black curve) and for a recessed electrode with $\gamma = 0.2$ ($r_a = 5$ μm, $d_p = 1$ μm) (red curve) (a); the normalized steady-state current as a function of the pore aspect ratio (b). (Color figure online)

The results on the electrode topology optimization formed the basis of the design of the biosensor chip prototype. The biosensor was realized as an on-chip packageless three electrode microelectrochemical cell, which includes a counter electrode (CE), an reference electrode (RE) and a working electrode (WE) patterned on a single silicon chip as shown in Fig. 8. The WE was located at the end of the chip to provide its separation from RE and CE. Such an arrangement was implemented in order to facilitate the bio functionalization chemistry and prevent both RE and CE from interference with this process. The chip size was 10.16 × 37.70 mm. To provide connectivity to the instruments the chip is equipped with 4 rectangular contact gold pads of 2.50 × 5.00 mm dimensions with a standard 2.54 mm pitch. The CE was made from platinum of 5.25 × 5.00 mm dimensions. The RE was a circular Ag/AgCl electrode of 1.00 mm diameter. The WE represents an array of microdisk or microband electrodes of different parameters as shown in the Table 2. The best results for the biosensor were obtained with the microdisc array with 40 μm diameter recessed gold disks, arranged in a hexagonal configuration with 400 μm center-to-center spacing which subsequently underwent surface modification as will be described below.

The on-chip micro electrochemical cell was fabricated at the Central Fabrication Facility at Tyndall National Institute. For fabrication of the chip was used a standard photolithography and lift-off techniques with different masks associated with the cell electrodes as schematically shown in Fig. 9 and previously discussed in [10, 24, 45]. In brief this process can be described as follows. Firstly, a silicon oxide layer of 1 μm thickness was thermally grown on the silicon substrate of N-Type, <111>-orientation and alignments marks were patterned on it. The selection of the substrate type is related to its high resistivity. Then the 20 nm thick titanium and 150 nm thick gold layers were patterned on the wafers to prepare for electrodes, connecting tracks and pads. The titanium layer acts as an adhesion layer, which improved the quality of the gold layer

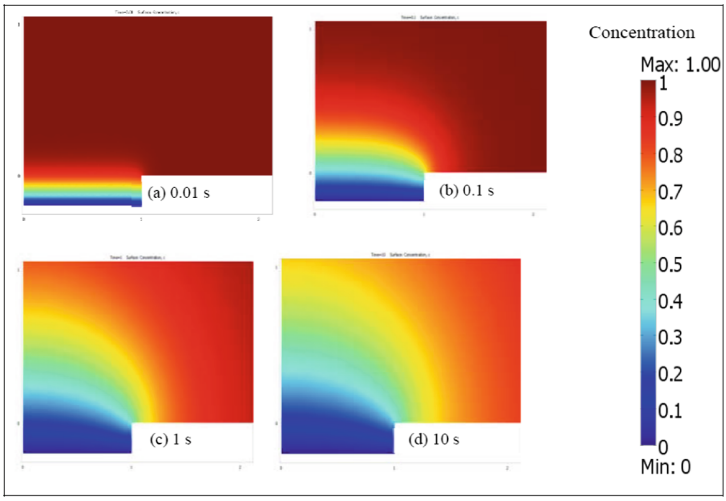

Fig. 7. Concentration distributions around the electrode for the recessed configuration electrode at the indicated times in s.

Table 2. Parameters of working electrode arrays.

Geometry	Disc diameter/ band width, μm	Band length, μm	Center-to-center separation, μm	Number of electrodes	Surface area, m^2
Disc	1	-	10	32592	2.56e−8
	5	-	50	1326	2.60e−8
	5	-	50	663	1.30e−8
	10	-	100	323	2.54e−8
	10	-	100	163	1.28e−8
	20	-	200	85	2.67e−8
	40	-	400	23	2.89e−8
Band	1	50	20	81	4.05e−9
	5	250	100	17	2.12e−8
	10	500	100	17	8.50e−8
	10	500	100	34	1.70e−7
	10	500	100	9	4.50e−8
	20	1000	400	5	1.00e−7
	40	2000	800	3	2.40e−7

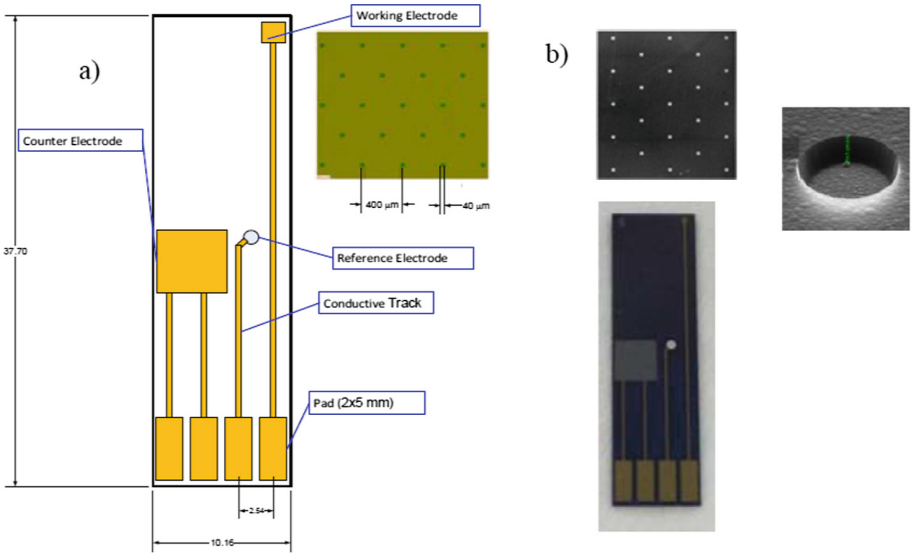

Fig. 8. Biosensor chip layout (a) and photos of fabricated chip, working electrode array and a single recessed microdisk (b).

deposit. Another 20 nm thick titanium adhesion layer was used before the deposition of the 150 nm thick Pt and of 250 nm thick Ag metals on the gold connection areas for the counter and reference electrodes where to promote the adhesion of Ag the Ti layer

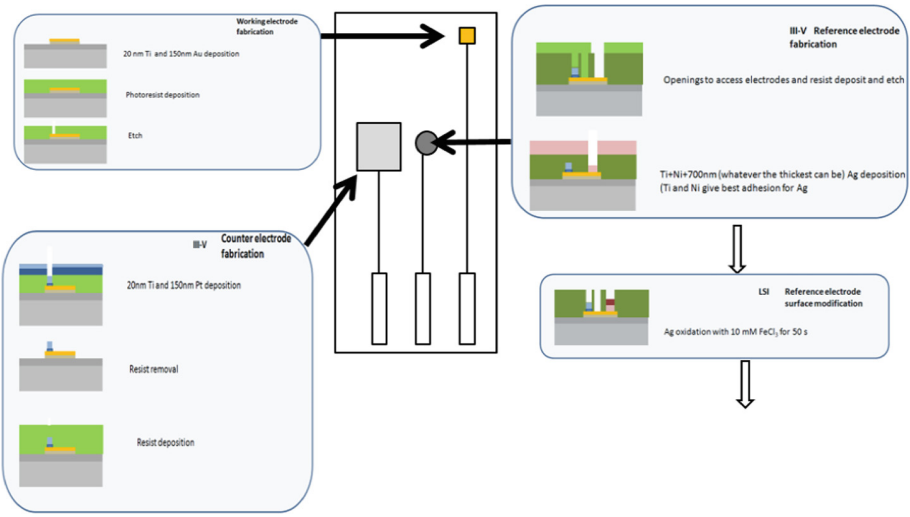

Fig. 9. Fabrication process for the three electrode on-chip micro electrochemical cell.

was supplemented by 20 nm of Ni. Then, 500 nm of silicon nitride was deposited on the whole wafer by plasma-enhanced chemical vapor deposition. The role of the silicon nitride is to insulate the connecting tracks from the solution. Openings for the electrodes and the connecting pads were obtained by plasma etching. Silver–silver chloride reference electrodes were prepared with help of chemical oxidation by immersion of the wafer in a 10 mM FeCl3 solution for 50 s. The metal was then lifted and a resist layer was spin coated on top of the wafer to protect the electrodes during the dicing of the wafer into individual chips.

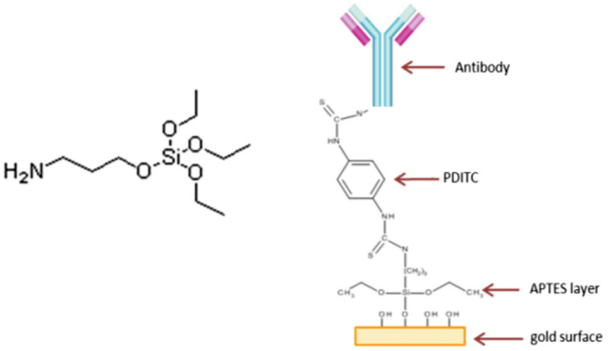

Fig. 10. Scheme of the electrode biofunctionalisation.

The required sensor specificity to the defined biotarget was introduced through application of a bio functionalization procedure which attached an antibody to the surface of a working electrode. Three surface modification techniques were

investigated including carboxymethyl dextran (CM-dextran) [46], and two silanisation based methods mainly (3-Glycidyloxypropyl) trimethoxysilane (GOPTS) with poly (ethylene glycol) (PEG) linker (GOPTS – PEG) [47] and (3-Aminopropyl)triethoxysilane (APTES) with 1,4-Phenylene diisothiocyanate (PDITC) linker (APTES - PDITC) [48].

The best results from the biosensor stability, reproducibility and sensitivity perspectives were obtained with APTES – PDITC methodology. This surface modification procedure is straight-forward and requires for its realization less time than two others that should be also referred to its merits. Here PDITC is a homobifunctional cross-linker containing two amine reactive isothiocyanate groups on a phenyl ring. Reaction with the amine group on silanised surface forms a thiourea linkage leaving the second isothiocyanate group free to couple with amine groups on the antibody (Fig. 10). This allows PDITC layer plays role of effective antibody cross-linker on APTES modified surface [49].

This procedure consisted of the following steps: Pretreatment, Silanisation, Activation and Biofunctionalisation that can be briefly described as follows [24, 40].

Pretreatment: The fabricated gold on silicon electrode chips are stayed in oxygen plasma cleaner for 10 min. Then, they are placed in Hydrogen chloride – methanol (HCl:MeOH, 1:1, v/v) solution for 15 min. After they are sonicated in acetone and isopropyl alcohol for 5 min each and finally are carefully rinsed in DI water and dry under a stream of nitrogen.

Silanisation: The treated chips are immersed in 3% APTES in MeOH:DI water (19:1) solution for 30 min at room temperature. Then the chips are rinsed with MeOH and DI water before left to be cure in the oven (dust free) for 15 min at 120 °C.

Activation: Following the curing step, the silanised WE are immediately drown in 18 mL of DMF solution containing 2 mL of 10% pyridine and 0.098 g 1,4-phenylene diisothiocyanate (-PDITC) (produces 25 mM PDITC) for 2 h for PDITC cross-linker attachment. Then the electrodes are carefully washed with DMF and DCE and dry under N2.

Biofunctionalisation: For antibody immobilisation anti-T2 toxin antibody was diluted in 0.1 M sodium borate pH 9.3 and the working electrodes were immersed in 100 μL of diluted antibody solution for 2 h at RT, wrapped in aluminium foil. Then the electrodes were removed, rinsed with DI water and dried with N2. All modification steps involving the chip treatment in the surface modification reactants are performed in such way that only the surface of working electrode (WE) is staying in contact with the solution to prevent contamination of other electrode on the chip.

2.3 Instrumentation

Instrumentation architecture implements impedance spectroscopy technique and represents low noise, highly sensitive measurement unit (analog part) under microcontroller control (digital part). The hardware provided stimulus signal, the front-end control, conditioning of the biosensor signal, its amplification, filtration, frequency transformation, data acquisition and communication with a control embedded

computer. The instrumentation implements the technique, which is known as electrochemical impedance spectroscopy (EIS) [50, 51]. It uses complex sensor impedance values (real and imaginary impedance components) obtained in a wide frequency range of the stimulation signal for analysis of the biosensor interfacial behaviour. The simplified block-diagram of the circuitry that provides measurement of real and imaginary components of the biosensor impedance Z_S is shown in Fig. 11.

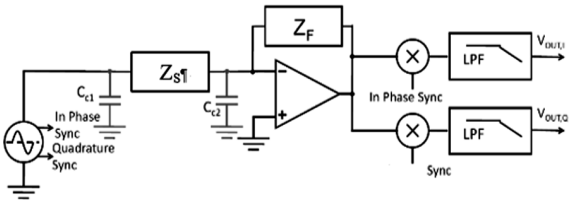

Fig. 11. Simplified block-diagram of impedance measurement circuitry.

It contains a stimulation signal source, which provides in-phase and quadrature AC signals, a transimpedance amplifier with feedback impedance Z_F and two (in-phase and quadrature) detection channels each consisted of a mixer and a low-pass filter. The output of the impedance measurement circuitry includes two DC signals, which contain information on biosensor complex impedance. Assuming that the multipliers have a unitary conversion gain the DC signals can be expressed as follows

$$V_{OUT\_I} = -\frac{V_{STIM}}{2}\frac{|Z_F|}{|Z_S|}\cos(\varphi_S - \varphi_F) \tag{3}$$

$$V_{OUT\_Q} = -\frac{V_{STIM}}{2}\frac{|Z_F|}{|Z_S|}\sin(\varphi_S - \varphi_F) \tag{4}$$

where V_{OUT_I} and V_{OUT_Q} are the output voltages of the two signal paths, V_{STIM} is the amplitude of the stimulation voltage; Z_F is the feedback complex impedance with module $|Z_F|$ and phase φ_F; Z_S is the sensor complex impedance with module $|Z_S|$ and phase φ_S. From the measured output voltages and the known feedback impedance the module and phase of the sensor impedance Z_S can be calculated as defined below

$$|Z_S| = -\frac{V_{STIM}}{2}\frac{|Z_F|}{\sqrt{V_{OUT\_I}^2 + V_{OUT\_Q}^2}} \tag{5}$$

$$\varphi_S = \arctan\left(\frac{V_{OUT\_Q}}{V_{OUT\_I}}\right) - \varphi_F \tag{6}$$

The method of signal extraction, which is used here, is called the lock-in technique. The advantage of this method is the reduction of impact of transimpedance flicker (*1/f*) noise on the measurement. This is because the noise in this technique can be reduced

by a final low-pass filter. Thus, if this filter has a narrow bandwidth, only the noise around the measurement frequency will influence the measurements.

The instrumentation architecture implemented in the system is shown in Fig. 12.

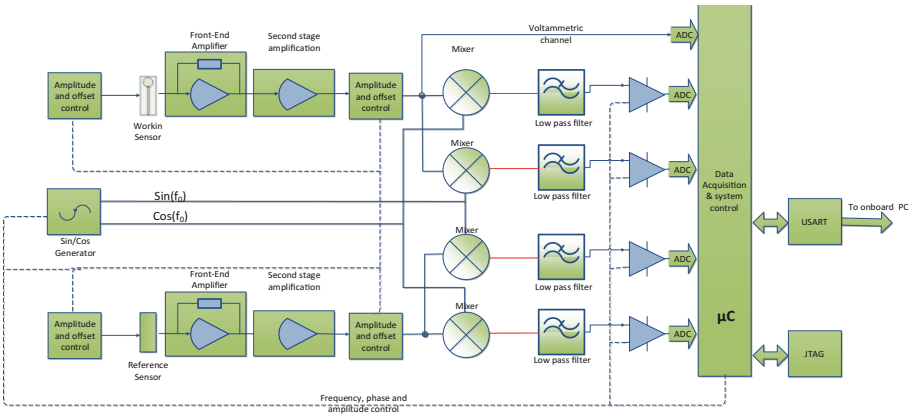

Fig. 12. Instrumentation architecture.

It represents a two channels impedance measurement system with a common signal generator providing in-phase and quadrature AC signals. Each channel includes a current to voltage converter (transimpedance amplifier) and two (in-phase and quadrature) demodulators, each is consisted of a mixer and a low-pass filter, and a level-shift circuit realised on the base of I^2C controlled DAC as shown in Fig. 13. The level-shift circuit is designed to match the sensor double polarity signal with a single polarity microcontroller analog to digital converter (ADC) and to facilitate fine module tuning and calibration. These two detection paths are a sensor channel for the actual measurement and a reference channel to compensate for the background signal.

The sensor connected to the reference channel should be not specific to the target analyte thereby capable of providing information on the sensor background signal resulting from varying parameters such as temperature, pH, nonspecific binding etc. If the background signal is of negligible value, the reference channel can be used as the second sensing channel for another bio target. It is based on the measurement technique

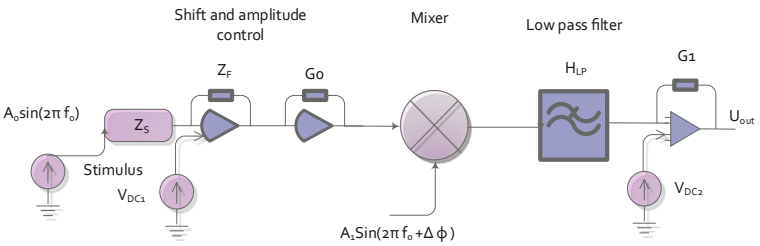

Fig. 13. Block-diagram of the measurement channel.

described above but has some additional features to facilitate its practical implementation. A known AC voltage that is generated by the signal generator is applied across the sensor and the current is converted to a voltage by the transimpedance amplifier. The voltage is amplified and demodulated in the I/Q demodulator yielding real and imaginary impedance components as described above. To increase the dynamic range of the module, 2-bit electronically controlled instrumentation amplifiers are included in the system structure after the transimpedance amplifier.

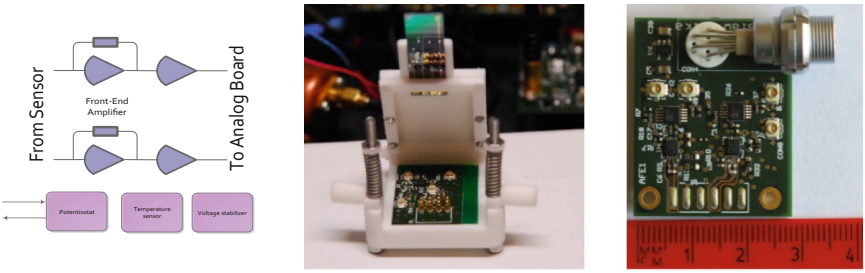

Fig. 14. Block diagram of potentiostat and front-end amplifiers module (a) and photographs of the packaged unit with the sensor chip (b) and the unit PCB (c) (photographs are taken from [24]).

The biosensing system hardware is realized by two modules: Potentiostat and Front-End Amplifiers (PFEA) and Signal Processing and Microcontroller (SPM) units. The PFEA (Fig. 14) is designed as a separate small size unit in order to locate it close to a reservoir where the biosensor tests the sample solution. This shortens the length of the connection wires whose link the biosensor and front-end amplifier, therefore decreases the leakage current and attenuates the noise and electromagnetic interference. The PFEA unit consists of a potentiostat, a temperature sensor and two transimpedance amplifiers providing current to voltage transformation of the sensor and reference (calibration) signals. The potentiostat is realized on three operational amplifiers OPA2211. Two identical transimpedance amplifiers are assembled from OPAMP ADA4647 and instrumentation amplifier AD8253. The unit is implemented on a small four-layer PCB of 25 mm × 35 mm dimensions.

The Signal Processing and Microcontroller (SPM) unit includes mixing and Analog Signal Processing (ASP), microcontroller and peripheral (μC) and Power Supply (PS) blocks. These three blocks forming the main body of the instrumentation are implemented in three separate 4 layer FR4 PCBs of 51 mm × 90 mm dimensions, which are integrated in a stack manner taking 55 mm of height as shown in Fig. 15.

The ASP block consists of Input, Switch, Level-Shifter and four identical Mixer/Low Pass Filter (LPF) lock-in circuits, which form two identical analog processing channels. Four-channel 16-bit digital to analog converters (DAC) incorporated into the SPM circuit is used to adjust DC levels in the SPM unit. The block was assembled from AD630 (Mixer), UAF42 (Low Pass Filter), ADG1419 (Switch), DAC8574 (DAC with buffered voltage output and I^2C compatible two wire serial

interface), AD8253 (Instrumental amplifier with 2-bit electronically controlled gain) and LM4140 (1.024 V voltage reference). The μC block is based on a high performance 8-bit ATxmega128A1U microcontroller. It realizes functions of instrumentation control, data acquisition and communication. It also contains the signal generator and four 16-bit DACs. The signal generator is based on AD9854 chip, which is a DDS synthesizer capable of parallel generation of precision sine and cosine signals in a wide frequency range. The SPM unit contains JTAG interface that allows in-circuit system programming and debugging. The PS block supplies stabilized low noise voltages of +8 V, −8 V, +3.3 V and −3.3 V to power the signal generators, microcontroller, ASP and PFEA system units. The PS block can be powered from a voltage source in the range of +5 V–+12 V.

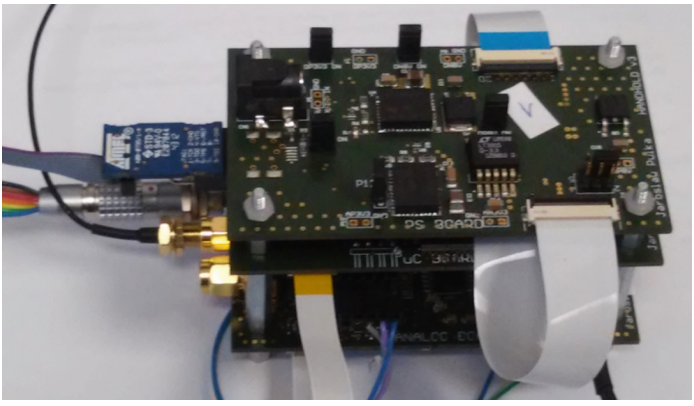

Fig. 15. Photograph of signal processing and Micro-controller unit (the photograph is taken from [24]).

2.4 Signal Processing and Corresponding Software

The associated instrumentation software consists of two highly interrelated parts written for a host computer and an ATxmega128A1U Atmel microcontroller. The software supports communication between the instrumentation and the computer, provides control of the hardware settings and its operation, implements biosensor impedance measurements, their signal processing and the target concentration determination. The computer software is realised with option of a user-friendly multi-tab GUI software that will be described below. Here each tab associated with the program window contains means for solutions of assigned tasks. There are three tabs/windows, namely 'Protocol', 'System configuration', and 'EIS'.

The tab/window '**Protocol'** shown in Fig. 16 is intended for careful design of frequency sweep protocol at each frequency point by applying values of frequency and a repetition number with possibility of adjustment all electronically controlled hardware parameters associated with the impedance measurements. As well all cells in the table including the frequency value can be edited to provide an individual trimming of

the measurement mode at the selected frequency. Two command buttons in the upper right corner allow for populating the table with default values (the upper large button) or with parameters, which are set in the SpinEdit controls (the lower small button) for a fast filling of table with the sweep parameter and hardware settings. Sweep parameters include the start *Fmin* and finish *Fmax* frequencies and a number of frequencies per decade, which are used to calculate frequency values distributed between *Fmin* and *Fmax*. Hardware settings duplicate the tuning parameters from the Hardware Configuration panel that will be discussed below. Accurate adjustment of the sweep parameters at each table raw (frequency) is available with the help of the SpinEdit control that can be activated in each cell. Frequency is tuned between the neighboring values in the table; hardware settings are limited by the corresponding hardware specification. The created Protocol table can be saved in the Excel file and conversely downloaded from the file.

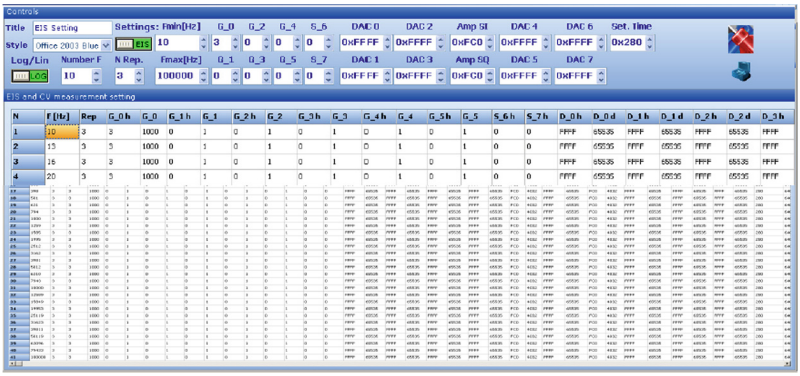

Fig. 16. Screen short of Protocol tab/window.

The tab/window '**System configuration'** shown in Fig. 17 supports communication control including received and transmitted data stream visualization, detection and control of communication and stream errors, data extraction from communication stream, instrumentation and measurement settings control and configuration and system operability testing. Tools for operability testing include Self-Test command, which starts Self-test measurement procedure followed by reporting about the measurement results in the 'Test parameters' plot and in the 'Test parameters' table in 'Hardware Configuration' panel. The program monitors these parameters before each impedance spectrum measurements that allows for easy identification of the hardware and the biosensor operability problem.

The tab/window '**EIS'** is the main instrumentation software part designed to provide all raw impedance measurements and corresponding signal processing and to present the obtained results in different forms as shown in Fig. 18. These include raw sensor impedance measurements presented by Nyquist (Imaginary impedance part vs. Real impedance part - 'Zim vs Zre') and Bode (Imaginary impedance part vs.

Frequency - 'Zim vs F', Real impedance part vs. Frequency - 'Zre vs F' and Phase vs. Frequency - 'Phase vs F') plots as well as the processed Nyquist spectra obtained after Kernel smoothing and subtraction of the reference background spectrum from the measured spectra with analytical signal extraction (see the plot 'Zim vs Zre processed' where the analytical signals extracted are highlighted by red points on the corresponding processed impedance spectra) and calculated analyte concentration in respect to the biosensor calibration (plot 'Anal. Signal vs. Concentration') in both graphical and table forms.

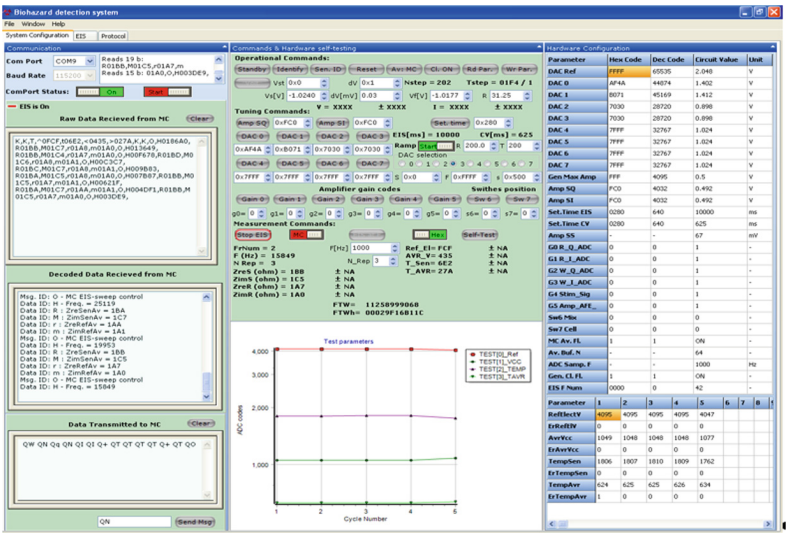

Fig. 17. Screen short of System configuration tab/window (the image is taken from [24]).

The measurements of imaginary *Zim*, real *Zre*, phase *Ph* values of the sensor impedance is based on the Eqs. (3)–(6) and the corresponding module calibration. For determination of the target concentration the special algorithm was developed. It is based on analysis of equivalent circuit of the electrochemical biosensor followed by experimental validation of the approach. The most used model for analysis of impedimetric biosensors is the modified Randles equivalent circuit [52] shown in Fig. 19. It includes resistor *Rs* that represents the resistance of the sample solution, in which the biosensor is immersed, and the resistance of the working electrode itself and the contacting track connecting the electrode with a corresponding pad presented an external electrical contact of the biosensor; capacitor C_D that arises from the series combination of several capacitive elements, such as analyte binding (C_{An}) to a sensing layer (C_{Se}) on an background electrode (C_{Bg}) capacitances; charge transfer resistor *Rct* that comprises the series connection of resistors incorporating the analyte binding (R_{An}) to a sensing layer (R_{Se}) on an electrode (R_{Bg}) and diffusion impedance Z_D whose frequency behaviour depends on the electrode system structure, shape and size of its elements [53]. The C_{An} capacitance is most sensitive to binding of large species, such

Fig. 18. Screen short of EIS tab/window (the image is taken from [24]). (Color figure online)

as proteins or cells. One difficulty with capacitive based sensors is that their sensitivity depends on obtaining the proper thickness of the sensing layer [54]. The charge transfer resistor *Rct* can also be quite sensitive to analyte binding, particularly in case of large species, such as proteins or cells, which significantly impede electron transfer.

It was found that for any (macroelectrode, microdisk or microband array) implementation of the biosensor transducer and any mechanism of manifestation of biorecognition reaction through changes in charge transfer resistence or sensor capacitance, the best results can be obtained through application of a differential measurement scheme, realized by subtracting the reference spectrum from the measured impedance spectrum. In this case the measured spectrum is the biosensor impedance spectrum after reaction with the target analyte and the reference spectrum is the biosensor impedance spectrum before reacting with the target analyte or an impedance spectrum obtained from the reference sensor if the last presents in the system. After subtraction, the maximum value of the imaginary part of the differential impedance spectrum can be taken as an analytical signal in the biosensor calibration step and also determination of the target analyte concentration. Using this quantity as an analytical signal instead of such equivalent circuit parameters as C_D or R_{ct} makes the signal processing algorithm straightforward, thus it does not require high calculation power from the control computer for its implementation. Additionally, this impedance spectrum value is located in the middle of the frequency sweep. It reduces requirements on the desired sweep range and therefore simplifies the hardware realization that is also very important for the portable devices. Overall, the application of a differential measurement scheme allows an increase in sensitivity and a reduction in the background signal. At the same time this approach suffers from noise. The injurious effects

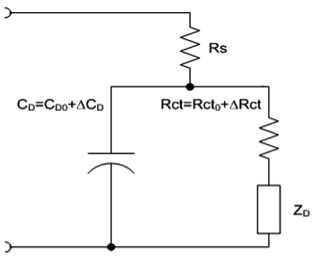

Fig. 19. The modified Randles equivalent circuit for biosensor analysis.

of noise can be reduced by both signals undergoing smoothing before their subtraction. Different smoothing approaches including median, adaptive and Gaussian kernel smoothing algorithms were tested to find the procedure that fits application specification in the best way. It was found that Gaussian kernel smoothing method provides required noise suppression and meets application requirement on simplicity and low power of calculation. Since the window based smoothing methods start working effectively only after the smoothing window is fully filled with samples the suggested approach does not work in the beginning and at the end of the impedance frequency sweep. This disadvantage is not critical in our case as the extracted parameter selected as the analytical signal is located in the middle of the frequency sweep and this limitation does not it affect.

2.5 Method and Chemicals

All electrochemical experiments were performed in a Faraday cage, and each measurement used for obtaining sensor calibration was carried out three times. EIS measurements were performed with the described system over a frequency range from 10 Hz to 100 kHz at an applied potential of DC bias of 0.2 V and an AC amplitude of 10 mV. The frequency range was defined by hardware specification and application objective to determine analyte concentration. The appropriate bias potential was determined from cyclic voltammetry over a range 0 V to 0.6 V at a scan rate of 100 mV/s. All chemicals used in this work including T2-toxin and corresponding antibodies were purchased from Sigma Aldrich Ireland Ltd. and used as received.

3 Results and Discussion

The developed portable immunosensing impedimetric system and suggested approach for the analytical signal extraction was validated with experimental data obtained with T2-toxin in the concentration range of 0–250 ppb. The transducer topology that produced the best sensing result for immunosensor prototype with APTES-PDITC biofuntionalisation chemistry described above and applied to the 40 μm microdisk array with parameters as indicated in Table 2. Experimental raw and smoothed and differential impedance spectra (in the Nyquist form) obtained with the developed biosensing system for different T-2 toxin concentrations (0, 25 ppb, 50 ppb, 100 ppb, 250 ppb)

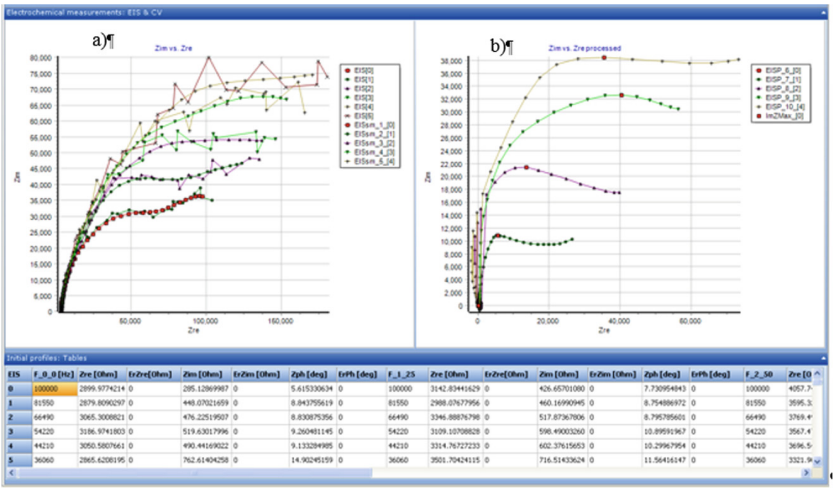

Fig. 20. Experimental raw and smoothed (a) and processed differential impedance spectra with extracted analytical signals (red points) (b) obtained with the developed biosensing system for different T-2 toxin concentrations (0, 25 ppb, 50 ppb, 100 ppb, 250 ppb). (Color figure online)

can be seen in screenshot presented in Fig. 20. In order to provide better spectra distinguishability the measurements were made without repetitions thus zero measurement errors are shown in the corresponding table below the plots. Due to a relatively high low boundary of the frequency sweep (10 Hz) the obtained impedance spectra accounted only for high and middle frequency parts of a depressed semicircle response of a microdisc electrode array associated with semi-infinite radial spherical diffusion. When concentration of T2-toxin increases, real and imaginary impedance parts both also increase that reflects a growth of a layer with targeted species captured by antibodies due the antibody-antigen binding reaction. If toxin concentration exceeds the certain level, this impedance increase is saturated due to a depletion of the free antibodies capable of biorecognition reaction. The raw impedance spectra were subjected to noise impact and application of Kernel's smoothing algorithm allowed for

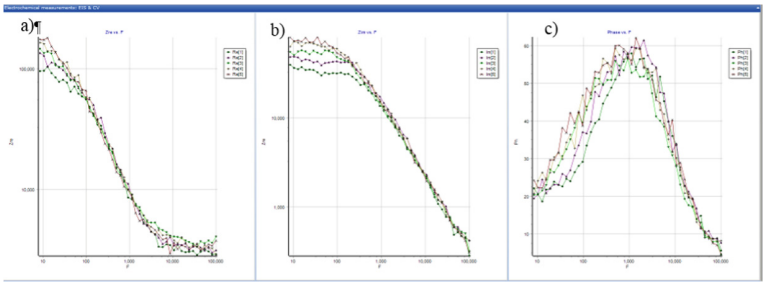

Fig. 21. Experimental smoothed Bode plots for real (a), imaginary (b) and phase (c) of the immunosensor obtained with the developed biosensing system for different T-2 toxin concentrations (0, 25 ppb, 50 ppb, 100 ppb, 250 ppb).

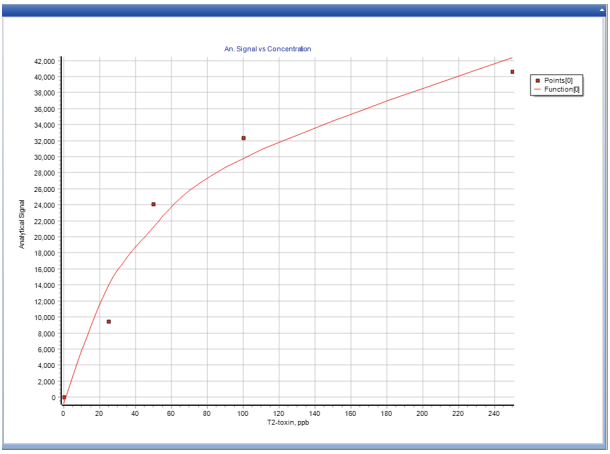

Fig. 22. Calibration curve of the immunosensor obtained with the developed biosensing system with five T-2 toxin concentrations (0, 25 ppb, 50 ppb, 100 ppb, 250 ppb). (Color figure online)

effective noise suppression. As was mentioned above the Kernel's smoothing cannot not work in the beginning and the end of the frequency sweeping that explains the signal oscillation in the plot with the smoothed differential spectra at high frequencies (area of the small impedances in Fig. 20b). At the same time since for the analytical signal are taken the maximal value of the imaginary part of the impedance located fare away from this zone this attribute of the smoothing method does not affect its measurement.

As follows from the smoothed Bode plots presented in Fig. 21 the most significant difference between the spectra corresponding to the different toxin concentrations is located in a low frequency range below 250 Hz. Here, the imaginary impedance values are more than 2 times less than their real counterparts (80000 vs. 180000); they are also more sensitive to variation of T2 toxin concentration. If frequency increases, both impedance components decrease but the imaginary impedance stays relatively constant at the frequencies below 250 Hz where the influence of the toxin concentration on the biosensor impedance is most noticeable. This frequency behavior of the imaginary impedance of the biosensor leads to the fact that frequency dependence of the impedance phase represents unimodal smooth function with maximal values in the range of 56–62° around the frequency of 1 kHz. The dependence of imaginary impedance against toxin concentration becomes more apparent from the differential impedance spectra obtained by subtraction of the spectrum at zero concentration, which is used as the reference background spectrum, from the impedance spectra corresponding to nonzero toxin concentrations as demonstrated in Fig. 20b.

The maximum values of the imaginary impedances on the differential impedance spectra marked by red points in this figure were used as the analytical signals to build a calibration curve of the developed label-free impedimetric immunosensor. This curve together with the analytical signals automatically extracted from the smoothed differential impedance spectra presented by the red squares is shown in Fig. 22.

The calibration curve represents a nonlinear function that reflects the competitive nature of the antibody-antigen binding reaction. The model can be presented by Eq. (7)

$$y = a \ln(x + b) + c \tag{7}$$

where y is analytical signal, x is T-2 toxin concentration. Other parameters of the model were determined by fitting the model with obtained experimental data. The following values of these parameters were attained slope $a = 2.667 \cdot 10^4$, $b = 22.449$ and $c = -8.393 \cdot 10^4$. The squared determination coefficient $R^2 = 0.982$ and the total approximation error was $3.929 \cdot 10^3$. As follows from the calibration curve, the developed biosensing portable system can successfully detect biotoxin at the levels below 25 ppm.

4 Conclusions

World-wide increase in bioterrorism activities has led to a corresponding focus on the available tools and techniques that can be deployed in the monitoring of biowarfare agents in the environment. The majority of technologies reside in a lab setting or have been boxed into a benchtop instrument with minimal or no portability possibilities. Portability leads to the potential to deploy at various points-of-need and currently, very few options exist. This paper presented a portable biosensing platform for impedance based detection and quantification of biotoxin substances capable of operation in autonomous mode has been developed. This has been made possible through the incorporation of cutting edge technologies from various disciplines e.g. sensor chip design and fabrication, application of surface chemistry approaches to develop a hybrid sensor chip with biotarget detection capabilities, highly miniaturized instrumentation, and the development of signal processing and data interpretation algorithms. The platform implements a label-free approach, which is based on detection of the biosensor interfacial changes due to a bio recognition reaction. The interfacial changes are sensed by means of Electrochemical Impedance Spectroscopy (EIS) in a frequency range from 10 Hz to 100 kHz. Traditionally, EIS instrumentation has been a relatively large, lab based piece of equipment due to its complexity in the generation of waveforms over a range of frequencies. corresponding data acquisition of the generated waveforms, and determination of the Nyquist/Bode plots. Advances in chip technology and embedded computing have now lead to increased functionality being possible in highly miniaturized off-the-shelf chips, and it is these advances that are incorporated here. The platform comprises of an electrochemical biosensor, portable low-noise mix signal hardware with embedded microcontroller and associated software incorporating hardware and measurement control together with signal processing algorithms for extraction biotarget concentration from the biosensor response. The biosensor is realized as an on-chip package-free three electrode micro electrochemical cell consisted of a Pt counter electrode, an Ag/AgCl reference electrode and an Au working electrode patterned on a single silicon chip. The WE represents an array of 40 micron diameter gold disks with 400 micron center-to-center distance, which were undergone of surface modification for antibody immobilisation. The surface modification was based on

APTES – PDITC procedure. The instrumentation was realised as a two channel EIS system, which used in-phase and quadrature demodulation of AC signal for extraction of the real and imaginary impedance components. The biosensing system hardware consisted of two modules: Potentiostat and Front-End Amplifiers (PFEA) and Signal Processing and Microcontroller (SPM) units. The corresponding software capable of autonomous operation contains two interrelated parts written for the host computer and the embedded microcontroller. An automated procedure for analytical signal extraction consists of: smoothing of the initial biosensor impedance spectrum by Kernel smoothing procedure; subtraction of a reference background spectrum from the measured impedance spectrum; and extraction from differential impedance spectrum the maximum of the imaginary component, which is used as an analytical signal for biosensor calibration and calculation of the target analyte concentration. The PC software was implemented with the option of user-friendly multi-tab GUI software where each tab is associated with the program window. These are 'System configuration', 'Protocol' and 'EIS' tabs/windows. They provide communication, instrumentation and measurement setting control, and system operability testing; allow for design of impedance measurement protocol for each frequency sweep point; and present results of EIS and analyte concentration quantification in graphical and table forms. The developed biosensing system was validated with the developed on-chip T2 toxin biosensor. Calibration of the system was obtained for five toxin concentrations from 0 ppm to 250 ppm. It showed that the developed portable biosensing system can provide successful detection of the biotoxin at the levels below 25 ppm.

Acknowledgements. Financial support of this work by European Commission projects FP7-SEC-2011.3.4-2 "HANDHOLD: HANDHeld OLfactory Detector" and H2020-NMP-29-2015 "HISENTS: High level Integrated SEnsor for NanoToxicity Screening" is gratefully acknowledged.

References

1. Shriver-Lake, L.C., Ligler, F.S.: The array biosensor for counterterrorism. IEEE Sens. J. **5** (4), 751–756 (2005)
2. Ahmad, A., Moore, E.J.: Comparison of cell-based biosensors with traditional analytical techniques for cytotoxicity monitoring and screening of polycyclic aromatic hydrocarbons in the environment. Anal. Lett. **42**(1), 1–28 (2009)
3. Brennan, D., Lambkin, P., Moore, E.J., Galvin, P.: An integrated optofluidic platform for DNA hybridization and detection. IEEE Sens. J. **8**(5), 536–542 (2008)
4. Bryan, T., Luo, X., Bueno, P.R., Davis, J.J.: An optimised electrochemical biosensor for the label-free detection of C-reactive protein in blood. Biosens. Bioelectron. **39**(1), 94–98 (2013)
5. Zhang, W., Du, Y., Wang, M.L.: Noninvasive glucose monitoring using saliva nano-biosensor. Sens. Bio-Sens. Res. **4**, 23–29 (2015)
6. Wang, X., Lu, X., Chen, J.: Development of biosensor technologies for analysis of environmental contaminants. Trends Environ. Anal. Chem. **2**, 25–32 (2014)
7. Yong, D., Liu, C., Zhu, C., Yu, D., Liu, L., Zhai, J., Dong, S.: Detecting total toxicity in water using a mediated biosensor system with flow injection. Chemosphere **139**, 109–116 (2015)

8. Herzog, G., Moujahid, W., Twomey, K., Lyons, C., Ogurtsov, V.I.: On-chip electrochemical microsystems for measurements of copper and conductivity in artificial seawater. Talanta **116**, 26–32 (2013)
9. Ogurtsov, V.I., Twomey, K., Herzog, G.: Development of an electrochemical sensing system for environmental monitoring of port water quality to integrate on-board an autonomous robotic fish. In: Hashmi, S. (ed.) Comprehensive Materials Processing. Sensor Materials, Technologies and Applications, vol. 13, pp. 317–351. Elsevier Science, Oxford (2014)
10. Said, N.A.M., Twomey, K., Ogurtsov, V.I., Arrigan, D.W.M., Herzog, G.: Fabrication and electrochemical characterization of micro- and nanoelectrode arrays for sensor applications. J. Phys. Conf. Ser. **307**, 012052 (2011)
11. Thevenot, D.R., Toth, K., Durst, R.A., Wilson, G.S.: Electrochemical biosensors: recommended definitions and classification. Pure Appl. Chem. **71**, 2333–2348 (1999)
12. Scheller, F.W., Wollenbergera, U., Warsinkea, A., Lisdata, F.: Research and development in biosensors. Curr. Opin. Biotechnol. **12**, 35–40 (2001)
13. Vo-Dinh, T., Cullum, B.: Biosensors and biochips: advances in biological and medical diagnostics. Fresen. J. Anal. Chem. **366**(6–7), 540–551 (2000)
14. Hock, B., Seifert, M., Kramer, K.: Engineering receptors and antibodies for biosensors. Biosens. Bioelectron. **17**(3), 239–249 (2002)
15. Wollenberger, U.: Third generation biosensors - integrating recognition and transduction in electrochemical sensors. In: Gorton, L. (ed.) Biosensors and Modem Biospecific Analytical Techniques, pp. 65–130. Elsevier, Amsterdam (2005)
16. Koyun, A., Ahlatcıoğlu, E., İpek, Y.K.: Biosensors and their principles. In: Kara, S. (ed.) A Roadmap of Biomedical Engineers and Milestones. INTECH, Rijeka (2012)
17. Sharma, S., Byrne, H., O'Kennedy, R.J.: Antibodies and antibody-derived analytical biosensors. Essays Biochem. **60**(1), 9–18 (2016)
18. Byrne, B., Stack, E., Gilmartin, N., O'Kennedy, R.: Antibody-based sensors: principles, problems and potential for detection of pathogens and associated toxins. Sensors **9**(6), 4407–4445 (2009)
19. Perumal, V., Hashim, U.: Advances in biosensors: principle, architecture and applications. J. Appl. Biomed. **12**(1), 1–15 (2014)
20. Dodeigne, C., Thunus, L., Lejeune, R.: Chemiluminescence as diagnostic tool. A review. Talanta **51**, 415–439 (2000)
21. Jiang, X., Li, D., Xu, X., Ying, Y., Li, Y., Ye, Z., et al.: Immunosensors for detection of pesticide residues. Biosens. Bioelectron. **23**(11), 1577–1587 (2008)
22. Yalow, R.S., Berson, S.A.: Assay of plasma insulin in human subjects by immunological methods. Nature **184**, 1648–1649 (1959)
23. Patel, Pd.: (Bio)sensors for measurement of analytes implicated in food safety. A review. Trends Anal. Chem. **21**(2), 96–115 (2002)
24. Ogurtsov, V.I., Twomey, K., Pulka, J.: A portable sensing system for impedance based detection of biotoxin substances. In: 10th International Joint Conference on Biomedical Engineering Systems and Technologies Proceedings, BIODEVICES, (BIOSTEC 2017), Porto, Portugal, vol. 1, pp. 54–62 (2017)
25. Sadana, A.: Biosensors: Kinetics of Binding and Dissociation Using Fractals, 1st edn. Elsevier, Amsterdam (2003)
26. Zhang, S., Zhao, H., John, R.: Development of a generic microelectrode array biosensing system. Anal. Chimica Acta **421**(2), 175–187 (2000)
27. Willner, I., Katz, E., Willner, B.: Layered functionalized electrodes for electrochemical biosensor applications. In: Yang, V.C., Ngo, T.T. (eds.) Biosensors and Their Applications. Elsevier, Amsterdam (2000)

28. Arrigan, D.W.M.: Electrochemical Strategies in Detection Science. Royal Society of Chemistry, Cambridge (2016)
29. Twomey, K., O'Mara, P., Pulka, J., McGillycuddy, S., et al.: Fabrication and characterisation of a test platform integrating nanoporous structures with biochemical functionality. IEEE Sens. J. **15**(8), 4329–4337 (2015)
30. Kafi, A.K.M., Lee, D.-Y., Park, S.-H., Kwon, Y.-S.: Potential application of hemoglobin as an alternative to peroxidase in a phenol biosensor. Thin Solid Films **516**(9), 2816–2821 (2008)
31. Zhou, Y., Tang, L., Zeng, G., Zhang, C., Xie, X., Liu, Y., Wang, J., Tang, J., Zhang, Y., Deng, Y.: Label free detection of lead using impedimetric sensor based on ordered mesoporous carbon–gold nanoparticles and DNAzyme catalytic beacons. Talanta **146**, 641–647 (2016)
32. Rushworth, J.V., Ahmed, A., Griffiths, H.H., Pollock, N.M., Hooper, N.M., Millner, P.A.: A label-free electrical impedimetric biosensor for the specific detection of Alzheimer's amyloid-beta oligomers. Biosens. Bioelectron. **56**, 83–90 (2014)
33. Arrigan, D.W.M.: Nanoelectrodes, nanoelectrode arrays and their applications. Analyst **129** (12), 1157–1165 (2004)
34. Bennett, J.W., Klich, M.: Mycotoxins. Clin. Microbiol. Rev. **16**(3), 497–516 (2003)
35. Gupta, R.C. (ed.): Handbook of Toxicology of Chemical Warfare Agents, 1st edn. Elsevier, Amsterdam (2009)
36. Ler, S.G., Lee, F.K., Gopalakrishnakone, P.: Trends in detection of warfare agents detection methods for ricin, staphylococcal enterotoxin B and T-2 toxin. J. Chromatogr. A **1133**, 1–12 (2006)
37. Zheng, M.Z., Richard, J.L., Binder, J.: A review of rapid methods for the analysis of mycotoxins. Mycopathologia **161**, 261–273 (2006)
38. Pittet, A.: Keeping the mycotoxins out: experience gathered by an international food company. Nat. Toxins **3**(4), 281–287 (1995)
39. De Saeger, S., Van Peteghem, C.: Dipstick enzyme immunoassay to detect Fusarium T-2 toxin in wheat. Appl. Environ. Microbiol. **62**(6), 1880–1884 (1996)
40. Said, M., Azura, N.: Electrochemical biosensor based on microfabricated electrode arrays for life sciences applications. Ph.D. thesis, University College Cork (2014)
41. http://www.handhold.eu/
42. Britz, D., Strutwolf, J.: Digital Simulation in Electrochemistry, 4th edn. Springer, Cham (2016). https://doi.org/10.1007/978-3-319-30292-8
43. Hermes, M., Scholz, F.: Solid-state electrochemical reactions of electroactive microparticles and nanoparticles in a liquid electrolyte environment. In: Kharton, V.V. (ed.) Solid State Electrochemistry I: Fundamentals, Materials and Their Applications. WILEY-VCH Verlag GmbH & Co. KGaA, Weinheim (2009)
44. Guo, J., Lindner, E.: Cyclic voltammograms at coplanar and shallow recessed microdisc electrode arrays: guidelines for design and experiment. Anal. Chem. **81**(1), 130–138 (2009)
45. Said, N.A.M., Twomey, K., Herzog, G., Ogurtsov V.I.: Fabrication and characterization of microfabricated on-chip microelectrochemical cell for biosensing applications. In: Zaaba, S. K., Zakaria, S.M.M.S., Kamarudin, K., et al. (eds.) Asian Conference on Chemical Sensors 2015, ACCS 2015, vol. 1808, pp. 020032-1–020032-13. AIP, Melville (2017)
46. Masson, J.-F., Battaglia, T.M., Davidson, M.J., Kim, Y.-C., Prakash, A.M.C., Beaudoin, S., Booksh, K.S.: Biocompatible polymers for antibody support on gold surfaces. Talanta **67**(5), 918–925 (2005)
47. Haddada, M.B., Huebner, M., Casale, S., Knopp, D., Niessner, R., Salmain, M., Boujday, S.: Gold nanoparticles assembly on silicon and gold surfaces: mechanism, stability, and efficiency in diclofenac biosensing. J. Phys. Chem. C **120**(51), 29302–29311 (2016)

48. Vashist, S.K., Dixit, C.K., MacCraith, B.D., O'Kennedy, R.: Effect of antibody immobilization strategies on the analytical performance of a surface plasmon resonance-based immunoassay. Analyst **136**(21), 4431–4436 (2011)
49. Raj, J., Herzog, G., Manning, M., Volcke, C., Maccraith, B., Ballantyne, S., Thompson, M., Arrigan, D.: Surface immobilisation of antibody on cyclic olefin copolymer for sandwich immunoassay. Biosens. Bioelectron. **24**, 2654–2658 (2009)
50. Barsoukov, E., Macdonald, J.R. (eds.): Impedance Spectroscopy Theory, Experiment, and Applications, 2nd edn. Wiley, Hoboken (2005)
51. Lasia, A.: Electrochemical impedance spectroscopy and its applications. In: Conway, B.E., Bockris, J., White, R.E. (eds.) Modern Aspects of Electrochemistry, vol. 32, pp. 143–248. Kluwer Academic/Plenum Publishers, New York (1999)
52. Suni, I.I.: Impedance methods for electrochemical sensors using nanomaterials. Trends Anal. Chem. **27**(7), 604–610 (2008)
53. Jacobsen, T., West, K.: Diffusion impedance in planar, cylindrical and spherical symmetry. Elecrochimika Acta **40**(2), 255–262 (1995)
54. Hu, S.Q., Wu, Z.Y., Zhou, Y.M., Cao, Z.X., Shen, G.L., Yu, R.Q.: Capacitive immunosensor for transferrin based on an o-aminobenzenthiol oligomer layer. Anal. Chim. Acta **458**, 297–304 (2002)